# The Influences of Residual Stress on the Frequency of Ultrasonic Transducers with Composite Membrane Structure

**Seungmock Lee**
*Micro Device Center, Technology Research Institute of Osaka Prefecture*
*Ayumino 2-7-1, Izumi, Osaka 594-1157, Japan*
**Jong-Min Kim*, Young-Eui Shin**
*School of Mechanical Engineering, Chung-Ang University,*
*221 Heuksuk-dong, Dongjak-ku, Seoul 156-756, Korea*

Arrayed ultrasonic sensors based on the piezoelectric thin film (lead-zirconate-titanate : $Pb(Zr_{0.52}Ti_{0.48})O_3$) having composite membrane structure are fabricated. Different thermal and elastic characteristics of each layer generate the residual stress during the high temperature deposition processes, accomplished diaphragm is consequently bowing. We present the membrane deflection effects originated from the residual stress on the resonant frequencies of the sensor chips. The resonant frequencies ($f_r$) measured of each sensor structures are located in the range of 87.6~111 kHz, these are larger 30~40 kHz than the resultant frequencies of FEM. The primary factors of $f_r$ deviations from the ideal FEM results are the membrane deflections, and the influence of stiffness variations are not so large on that. Membrane deflections have the effect of total thickness increase which sensitively change the $f_r$ to the positive direction. Stress generations of the membrane are also numerically predicted for considering the effect of stiffness variations on the $f_r$.

**Key Words :** Stress, Resonant Frequency, Ultrasonic Sensor, Sensitivity, Membrane

## 1. Introduction

Microelectromechanical system (MEMS) technologies are used to perform the tasks of macroscopic devices at a fraction of the cost and with improved functionality and performance. Ultrasonic transducers using the piezoelectric PZT film and multi-layered integrated circuits have been widely researched for the distance recognition, biomedical-imaging, automotive sensing fields. Recently, silicon based composite membrane structures have been employed on the ultrasonic transducers for the device miniaturization and enhanced mechanical sensitivity. We have been investigated the ultrasonic imaging system, constructed with integrated phased array sensing elements, for the three-dimensional imaging (Mo et al., 2003). On the composite membrane structure fabrications, since the different thin films are laminated by the HT deposition processes, a significant residual stress is usually generated on the resultant structure which has an important effects on the mechanical and electrical properties of the sensor chips (Okuyama, 2001 ; Sengupta et al., 1998 ; Hwang et al., 2003). The composite membrane is generally operated in resonance mode which is primarily decided by those dimensions and elastic properties. Stiffness variations and shape deformations of the membranes by the HT fabrication processes have important effects on the resonance frequencies. The relations between stress and frequency have been usually applied on

* Corresponding Author,
**E-mail** : 0326kjm@cau.ac.kr
**TEL** : +82-2-820-5728; **FAX** : +82-2-814-9476
School of Mechanical Engineering, Chung-Ang University, 221 Heuksuk-dong, Dongjak-ku, Seoul 156-756, Korea. (Manuscript **Received** May 12, 2005; **Revised** December 4, 2005)

Copyright (C) 2006 NuriMedia Co., Ltd.

the vibrating reed technique which is generally used to obtain the film's Young's modulus. The structural $f_r$ is proportion to the stress generations (Harms et al., 1998). The bending stiffness of the constraining layers is often relatively large in the plane parallel to lamination, enhancing the potential for damping of vibration in the plane of laminated beams (Nayfeh, 0000). Given a combined structure, the derivations of effective moment are necessary from the different strain status of each constitutive thin films. Also, the combined strain and stress relations for a one-dimensional laminated beam should be extended to two-dimensional plate behaviors. We demonstrate the total residual stress generations of composite membrane structure originating from the HT processes, which will determine the stiffness variations. On the other hand, membrane deflections have the effect of total thickness increase which sensitively change the $f_r$ to the positive direction. Since these deflections are mainly originated by thermal expansion differences of each constitutive layer, HT processes and process temperature differences may be the essential factor on the frequency variations.

In this work, we examine the numerical relations between thermally induced stress and resultant resonance frequency of the ultrasonic transducers. Several arrayed sensor chips are fabricated with different structures and film thickness using the micro-machining process. For finding the natural frequencies of each structure (not occurred the membrane deflections and thermal stress), finite element modeling (FEM) analysis has been carried out. Also, on the basis of elastic relations between adjacent films in the composite membrane, thermally induced stress originated from the fabrication process and total effective moment solutions are numerically approximated. From these results, the effects of stress generation and membrane deflection on the frequency shifts of each device structures have been considered and compared the differences depending on each structure.

## 2. Experimental

Fabrication of multi-layered ultrasonic sensor chip was carried out with a 4-mask process. SOI (Silicon-On-Insulator) wafer (Si 2.0 $\mu$m/$SiO_2$ 1.0 $\mu$m/Si 300 $\mu$m) obtained from shin-etsu chemical corp. was used as substrate. Surface oxide layer of this was thermally grown at 1100℃ with ≈1 $\mu$m thick. Three type sensor chips are fabricated, each dimensions of those are shown in Table 1. Cross-sectional schematic diagram of each sensor structure is also shown in Fig. 1, and the 49 diaphragm elements of that are arrayed in one sensor chip. Lower (Pt/Ti) and upper electrodes (Pt) were deposited using RF sputtering with 220 nm (Ti : 20 nm) and 200 nm thickness, respectively.

The multi-layer PZT film was prepared by Sol-Gel derivations. The solution of lead-zirconate-titanate ($Pb(Zr_{0.52}Ti_{0.48})O_3$) obtained from Mitsubishi Material corp. was spin coated on the lower electrode at 500 rpm for 5 sec and at 4000 rpm for 20 sec. Each film was dried at 300℃ for 10 mins and every four layers were annealed at 600℃ for 10 mins in pure oxygen ambient. The resultant PZT film thickness was measured using the spectroscopic reflectometer film thickness measurement system, Model : NanoSpec M3000, Nanometrics Inc., these results are also represented in Table 1. Initially aimed thickness were 0.8 $\mu$m (OR1, OE1) and 1.6 $\mu$m (OR2), while it can be known that the resultant film thickness was somewhat deviated from those. XRD patterns of

**Table 1** Structures and dimensions of fabricated sensor chips

| Sample No. | Composite membrane constitution | Pt ($\mu$m) | PZT thickness (Å) | Pt/Ti ($\mu$m) | $SiO_2$ ($\mu$m) | Si ($\mu$m) | $SiO_2$ ($\mu$m) |
|---|---|---|---|---|---|---|---|
| OR1 (Oxide Removed) | Pt/PZT/Pt/Ti/$SiO_2$/Si | 0.2 | 15356 | 0.22 | 1 | 1.7 | — |
| OR2 | Pt/PZT/Pt/Ti/$SiO_2$/Si | 0.2 | 7402 | 0.22 | 1 | 1.7 | — |
| OE1 (Oxide Exist) | Pt/PZT/Pt/Ti/$SiO_2$/Si/$SiO_2$ | 0.2 | 14815 | 0.22 | 1 | 1.7 | 1 |

Copyright (C) 2006 NuriMedia Co., Ltd.

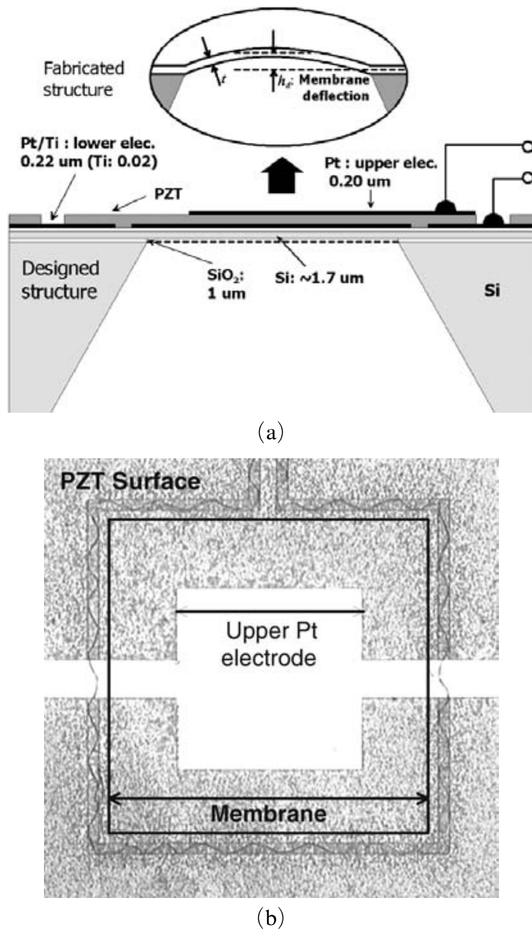


**Fig. 1** (a) Cross-sectional schematic diagram of sensor structure and (b) surface image fabricated. The membranes practically fabricated are deflected depending on the stress generations of each structure, which are measured by laser reflections and the results are listed in Table 3.

each PZT films showed perovskite phase having preferred (111) orientation. Lower silicon substrate of SOI wafer was anisotropically etched (wet-etching) using EPW (ethylenediamine-pyrocathecol-water) solution for making the arrayed diaphragm structure (see Fig. 1). Surface deflection of each diaphragm was measured using the laser reflection methode (Model: NH-3N, mitaka kohki Co.). Deflection dimensions of each specimen were averaged from the data of 49 elements. In the measurement system of resonant frequencies, sound pulse is generated by electrical discharge, and it's acoustic pressure is estimated as ~4.2 Pa at 1m distance. The output signals from the sensor device are amplified in the free amp and the relations of output intensity vs. frequency of those are given by Fourier transform.

## 3. Results and Discussion

### 3.1 Finite element modeling

The finite element method provides a graphic-oriented modeling and analysis tool that can be used to solve a wide variety of shock and vibration design analysis. It incorporates modeling structures that transform a complex model into a set of matrix equations of the form. Modal analysis has been used to interpret the resonant mode of the sensor structures, which has useful characteristics, like as a) it shows displacement maxima in a vibration behavior, and b) it reveals the frequencies of natural vibrations. We predict the natural frequencies of each fabricated structures, which are the ideal structures not having the thermal stress and membrane deflection. These will make possible to consider the $f_r$ deviations originated from the stress generations. ANSYS 7.1 has been used in this analysis, and 3-D modelings of three-type sensor structures are carried out with the same dimension as practically fabricated ones as shown in Table 1. Since the membrane has the symmetric rectangular structure, half of that was modeled as shown in Fig. 2 (a). The linear elastic properties of materials constructing the sensor structure are listed in Table 2, which are used in the FEM analysis. On the preprocess of modal analysis, all elements were meshed with 12-noded 3-D solid elements (solid 95). Symmetric boundary conditions are applied to the plane of symmetry. Zero displacements were applied in the $x$, $y$, and $z$ directions at the bottom of lower Si-membrane. The uniform acoustic pressure of 4.2 Pa was applied to the upper surface areas of the modeled structure, which is the same condition with the practical measurement. The matrix eigenvalue problem for a typical undamped Modal analysis is

Copyright (C) 2006 NuriMedia Co., Ltd.

given by

$$[K]\{\phi_i\}-\omega_i^2[M]\{\phi_i\}=\{0\} \quad (1)$$

where $[K]$ is the structure stiffness matrix and $\{\phi_i\}$ is the eigenvector representing the mode shape of ith natural circular frequency. $\omega_1$ represents the ith natural angular frequency, and $[M]$ is defined as mass matrix. The Block Lanczos method was chosen for finding the natural frequencies. Inertia and damping forces did not considered in this analysis.

The resultant natural frequencies of each structure are summarized in Table 3, and 1st mode shapes are also shown in Fig. 2(b). The 1st mode frequencies are located in the range of 55∼70.8 kHz depending on each sensor structure. The resultant frequencies are principally determined by the dimensions and elastic properties of the constitutive layers of the membrane. In these three types of sensor structure, PZT film thickness and bottom $SiO_2$ layer play an important role on the $f_r$ determinations. Although the elastic properties referenced could have differences with the practical ones, the influences on the $f_r$ are only several kHz order under the referenced error range. Since the $f_r$ differences between each structure did not changed, those results are sufficiently meaningful. The high mode (2nd and 3rd) frequencies of the Modal analysis could not be obtained in the practical measurements.

On the other hand, since the mode shapes represented in Fig. 2(b) is undamped behavior, those may be exaggerated than the practical vibrations. The stiffness variations originated by

**Table 2** Young's modulus, density, Poisson's ratio and thermal expansion coefficients of each layer

| Material | Young's modulus (GPa) | Poisson's ratio | Thermal expansion coefficient ($10^{-6}$℃$^{-1}$) |
|---|---|---|---|
| Si | 130[c] | 0.27[e] | 4.20[c] |
| $SiO_2$ | 66[d] | 0.17[f] | 7.00[d] |
| Pt | 147[a] | 0.39[a] | 8.90[b] |
| Ti | 110[g] | 0.31[g] | 9.00[b] |
| PZT | 63[h] | 0.3[a] | 4.10[c] |

[a] Reference 13. [c] Reference 15. [e] Reference 17. [g] Reference 19.
[b] Reference 14. [d] Reference 16. [f] Reference 18. [h] Reference 20.

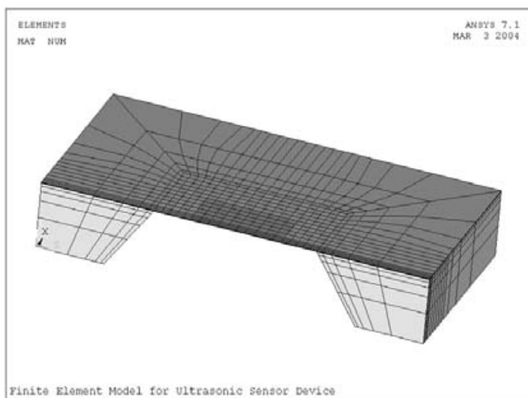


(a)

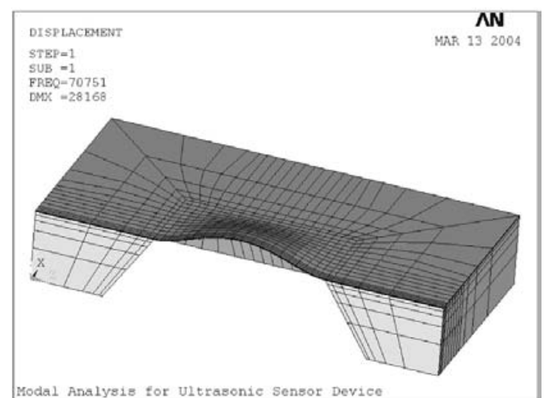


(b)

**Fig. 2** (a) 3-D modeling image of the sensor structure made with three types using the ANSYS 7.1. Those are the same dimensions with practically fabricated structures. (b) The undamped 1st mode shape of fabricated sensor structure carried out by the Modal analysis. High (2nd and 3rd) mode behaviors could not be obtained in the practical measurement.

Copyright (C) 2006 NuriMedia Co., Ltd.

**Table 3** Membrane thickness, deflection, FEM results and measured resonant frequencies

| Sample No. | Total membrane thickness ($\mu$m) | Membrane deflection $h_d$ ($\mu$m) | Ansys 1st Mode (kHz) | Practically measured $f_r$ (kHz) | $\Delta f_r$ (FEM-measured) (kHz) | *Calculated total stress $\left(\sum_{i=1}^{N}\frac{t_i\sigma_i}{t}\right)$ (Pa) |
|---|---|---|---|---|---|---|
| OR1 | 4.65 | 3.99 | 62.24 | 90.8 | 28.6 | $-1.14\times10^7$ |
| OR2 | 3.86 | 4.92 | 54.88 | 87.6 | 32.7 | $8.28\times10^7$ |
| OE1 | 5.60 | 7.95 | 70.75 | 111 | 40.3 | $-8.86\times10^7$ |

*Negative : Tensile stress
Positive : Compressive stress

thermal stress and membrane bending affect significantly on the active damping efficiency (Pietrzakowski, 2001), and structural and mechanical factors are principally important factors on the damping potential.

### 3.2 Resonant frequencies of each sensor structures

From the membrane vibrations originated by acoustic pressure (≈4.2 Pa), electric output signals and those FFT results of each structure are obtained (see Fig. 3), and the resultant RFs of each sensor chip are listed in Table 3. The $f_r$ of each structure is the mean value of 30 membrane elements those represented a good reproducibility. The measured $f_r$s are located in the range of 87.6～111 kHz, and principally proportion to the total membrane thickness, which are well consistent with the FEM results. These measured $f_r$s are larger 28.6～40.3 kHz than the FEM results of each corresponding structures. The $f_r$ difference between OR1 and OR2 is about 3.2 kHz, while that between OR1 and OE1 is 20.2 kHz which is remarkably larger than the former. In the FEM results, differences of OR1-OR2 and OR1-OE1 specimens are almost same as 7.4 kHz and 8.5 kHz, respectively. We consider that these differences are principally attributed to the membrane deflections and the stiffness variations originated from thermal stress. The relations between those have been considered. Firstly, the relations between stress and frequency could be derived as follows. When a system vibrates in a natural mode, the mode shapes of plates having various edge conditions give logical functions with which

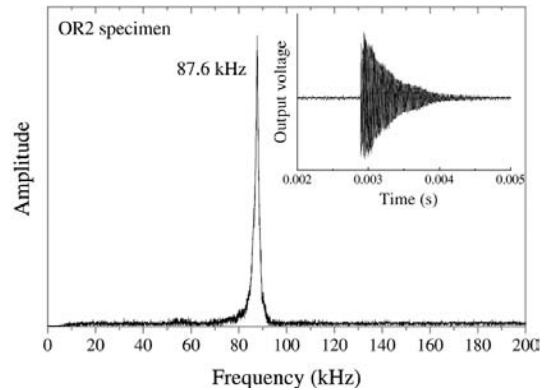


**Fig. 3** Frequency response of OR2 specimen given by Fourier transfer.

to formulate shapes for determining the natural frequencies by the Rayleigh and Ritz methods (Harris, 1995). To apply this method, finding the maximum strain ($V_{max}$) and kinetic energy values and equating them, and solving for angular frequency $\omega_n^2$ gives the following frequency equation:

$$\omega_n^2=\frac{2}{\rho h}\frac{V_{max}}{\iint W^2\,dxdy} \quad (2)$$

where $\rho$ is density and $h$ is thickness. $W$ is a function of $x$ and $y$, which is assumed that satisfies the necessary boundary conditions of the plate. D. Young et al.(Harris, 1995) solved this equation for the fundamental frequency of the rectangular plate clamped in all edges (membrane structure), that is expressed as

$$\omega=35.99\sqrt{\frac{D}{\rho t a^4}} \quad (3)$$

where $a$ is the $x(=y)$ axis dimension of mem-

Copyright (C) 2006 NuriMedia Co., Ltd.

brane and $t$ is the total thickness. $D=Eh^3/12(1-\nu^2)$ is the plate stiffness, $h$ being the plate thickness and $\nu$ Poisson's ratio. Due to the sensor chips having composite membrane structure, the total stiffness should be obtained by combining the constitutive layer's properties. $D$ in the Eq. (3) can be expressed as $K/(1-\nu^2)$, where $K$ is written as

$$K=\sum_{i=1}^{N} E_i I_i \tag{4}$$

where $E_i$ and $I_i$ is the Young's modulus and the moment of inertia of $i$-th layer. From the vibrating reed technique, the modulus change due to the stress generations of thin film in the case of rectangular sample cross-section could be derived (Harms et al., 1998) as given by

$$\Delta E=\frac{1-\nu_f^2}{1-\nu_s\nu_f}\left(\frac{1}{5}\frac{\sigma_f^2}{E_s}\frac{b^4}{d_s^4}\frac{d_f}{d_s}\right) \tag{5}$$

where $\sigma$ is stress, $b$ and $d$ is the length and thickness of the beam, with indices $s$ for substrate and $f$ for film. If Eq. (5) introduce to the Eq. (3) and (4), we can find that the stress influence on the frequency is proportion to $(\sigma^2(b/d)^4)^{1/2}$, which confirm that the natural frequency of a composite membrane structure is proportion to stiffness variations originated from the stress generations and the dimensions of membrane. So that the considerations of stress generations of each structure is essential on the $f_r$ variation. The HT fabrication processes make a substantial stress on each constitutive layer of the membrane. On the other hand, if a tensile force is generated, it is contribute to the strength of the plates by counteracting the bending according to the vibrations produced by lateral load these action increases with increasing the deflections (Pietrzakowski, 2001). So that a reduction of maximum tensile stress originated from the load can be accomplished by giving a suitable initial curvature to the membrane. These factors must be considered in the stress calculations. We predict the stress of each structures considering the HT processes of each constitutive layer and membrane bending, and those results are discussed relating to the $f_r$ results.

### 3.3 Thermal stress on the composite membrane

On the composite membrane structure, each thin film is deposited with the same linear dimension ($d_i=d_x$, $d_y$ : constant). The equilibrium condition of this composite layer is, (1) the dimensions of each layer must be the same at the interface, and (2) the internal resultant end forces and applied moment is zero. The strain contributions originating from a possible lattice mismatch between different films deposited are neglected on the stress calculations. From the boundary condition for coherent interfaces, the net strain origins between two adjacent layers can be described as a function of the magnitude of the thermal axial strain and bending strains originated from the plate curvature. On the composite layer having different Young's modulus, thermally induced stress in each layer can be expressed as (Townsend et al., 1987)

$$\sigma_i=\frac{E_i}{1-\nu_i}\left[-\alpha_i\cdot\Delta T+\left(\frac{\sum_j \frac{E_j t_j \alpha_j}{(1-\nu_j)}}{\sum_j \frac{E_j t_j}{(1-\nu_j)}}\right)\cdot\Delta T+(\pi-z)K\right] \tag{6}$$

where $\alpha_i$ is the linear thermal expansion coefficient of ith layer, $\Delta T$ describes the temperature difference between RT and deposition temperature of each layer. $K$ is composite curvature, $\pi$ is the position of the neutral plane, and $z$ is the coordinate distance normal to the linear dimension of composite layer. First two terms are corresponding to the axial strain, and the last one is bending strain. The location of the neutral plane can be determined by the repeated requirement of zero resultant end forces, which is defined as

$$\pi=\frac{t}{2}-\frac{\sum_{i=1}^{n} E_i t_i \gamma_i}{2\sum_{i=1}^{n} E_i t_i} \tag{7}$$

where $\gamma_i$ is given by $\gamma_i=\sum \beta_{ij} t_i$ and $\beta_{ij}=-1$ for $j<i$, 0 for $j=1$, and 1 for $j>i$. In the case of our membrane structures, since the linear dimensions of each layer are initially determined, the volume variation coming from the anisotropic etching of Si substrate should be substituted by its thickness

Copyright (C) 2006 NuriMedia Co., Ltd.

changing. The thermal stress on the membrane is independent of the position and uniformly distributed in the device, even if the Si substrate shape is formed irregularly. So that, a effective thickness is induced for compensating the substrate shape irregularity in modeling, which can be described as

$$V'_{Si}=\int_0^{t'_{Si}} d_x d_y dt = V_{Si}-V_{etched}$$
$$t'_{Si}=\frac{d_x d_y}{V_{Si}-V_{etched}} \quad (8)$$

where $V'_{Si}$, $V_{Si}$, $V_{etched}$ are the volumes of etched Si substrate (after etching), initial Si substrate (before etching) and anisotropically etched volume, respectively. $d_x$, $d_y$ are $x$ and $y$ linear dimensions, respectively, and $t'_{Si}$ is the resultant effective thickness of Si substrate. The $SiO_2$ layer of OR specimens are etched in the diaphragm portion, effective $SiO_2$ layer thickness, $t'_{SiO_2}$, also induced to the elastic strain considerations of that. The resultant stress sum of the constitutive layers can be calculated as

$$\sigma=\sum\sigma_i=\sum_{i=1}^{N}\frac{t_i\sigma_i}{t} \quad (9)$$

where $t$ is total thickness of membrane. The elastic and thermal properties used in the calculations are listed in Table 2 which are same with that used already in the FEM analysis, and the resultant stresses of each structure are shown in Table 3. OR1 and OE1 structures have tensile stress, while the OR2 has a compressive one. The axial strain of OR specimens were compressive, while the bending strain made the OR1 to tensile stress. Since the surface oxidation of SOI wafer is carried out at the highest temperature (≈1100℃), resultant total stress is principally determined by the stress generations of these portions. So that, the OE1 specimen has the highest tensile stress, in which the oxide inter-layer of SOI wafer is exist in the membrane, this probably leads to the largest $f_r$ difference between FEM result and measured one. The $f_r$ differences of each specimen are proportion to these stress sums of membrane (see Eq. (5)), while those are independent of force direction.

On the other hand, since the thermal oxidation of SOI surface and PZT deposition processes are carried out repeatedly at high temperature, initially generated stress is considered to be relaxed somewhat during those processes by annealing effect. According to the Maxwell model of a solid (Irene and Tierney, 1982; Fitch et al., 1989), stress relaxation occurs by viscous motion of the $SiO_2$ material away from the growth interface. In the Maxwell model for stress relief, the total stress relaxation can be expressed for the time and temperature dependence as described by (Irene and Tierney, 1982)

$$\sigma_i(t)=\sigma_i(0)\exp\left(\frac{-t}{\tau}\right)=\sigma_i(0)\exp\left(\frac{-tG}{\eta_0\exp(E_\eta/RT)}\right) \quad (10)$$

where $\sigma(0)$ is the maximum intrinsic stress at some position, and $t$ is the oxidation or annealing time. $G$ is the shear modulus and $\eta$ is the oxide viscosity. $\eta_0$ the minimum viscosity $E_\eta$ an empirical activation energy and $R$ is the gas constant. $\tau$ is viscoelastic relaxation time. Temperature dependence of the viscosity $\eta$ dominates over the fabrication process temperature range. Stress relief is consequently the exponential function of temperature and time. Fitch et al. (1989) reported that, at the $SiO_2$/Si interface, thermal stress of SOI wafer is remarkably changed by the fabrication process over the temperature of 1000℃, while the influence is not so large under the temperature. We consider that the stress generations and relaxations of PZT deposition processes carrying out at 600℃ for 10 mins have relatively minor effect on the total membrane stress comparing to that of SOI wafer fabrications.

### 3.4 Membrane deflection effects on the frequency shift

The initial membrane deflections have the effect of total thickness increase (Timosenko and Woinowsky-Krieger, 1959), which make the frequency change to the positive direction. From the Rayleigh method, symmetry and dimensional considerations show that the effect on frequency is proportion to $(L/R)^2$ and thus of the influence of

Copyright (C) 2006 NuriMedia Co., Ltd.

longitudinal curvature. Harms et al. (1998) derived the relations between the curvature of beam and frequency variations which is expressed as,

$$\frac{\Delta\omega^2}{\omega^2}=a\cdot\frac{L^2}{R^2} \tag{11}$$

where $L$ is the length of beam, $R$ is the radius of curvature for the lowest mode. In the case of composite membrane, frequency variations should be the function of longitudinal membrane curvatures since the lateral dimensions are initially determined. The $f_r$ differences between FEM and measured ($\Delta f_r$) are well consistent with this tendency, which are shown in Fig. 4 and Table 3. In that, remarkable increase of membrane deflection between OE1 and OR2 lead to the increase of the $\Delta f_r$ ($\approx$8 kHz), which is two times larger than that of OR1 and OR2 specimens, while the stress generations make not so large changes between those. It can be supposed that the substantial tensile stress of OE1 leads to the highest membrane curvature. Pietrzakowski et al. (2001) predicted that the influence of bonding layer elasticity on the dynamic response of the control beam bonded with piezoceramic actuator. In that, the stiffness parameter variations in the range of $10^{10}\sim5\times10^{12}$ $Nm^{-3}$ lead to the frequency shift of several Hz. We consider that the frequency variations originated from the stiffness variations due to the thermal stress may be several～several tens Hz range which can be negligible on the $f_r$ differences between FEM and measured results (see Table 3). Consequently, the frequency deviations from the FEM results are primarily originated from the membrane deformations. Although there are probably some neglected non-structural factors influencing on the vibration such as variations in phase composition and microstructure of PZT layer, the influence of these on the $f_r$ can be negligible.

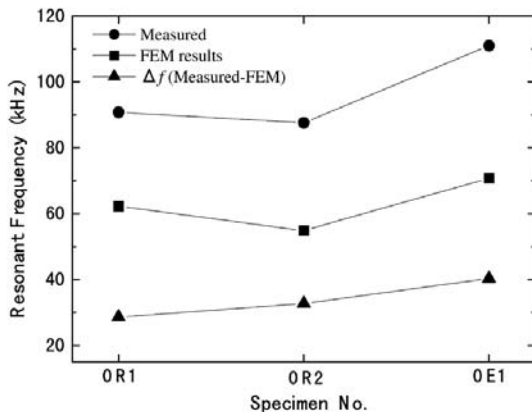


**Fig. 4** Resonant frequency results of FEM, practically measured and the differences between these of each structure. The measured $f_r$s are the mean value of the 30 membrane elements which represented a good reproducibility.

The frequency deviations from the FEM results are substantial on the resultant $f_r$, meaning that the thermal stress and membrane deflections of each structure should be the primary consideration factors on the sound source, frequency and structure designs on the ultrasonic sensor fabrications.

## 4. Conclusions

Thermal stress and membrane shape deformation effects on the resonant frequency of ultrasonic transducers having composite membrane structures are demonstrated. On the FEM results, the film dimensions mainly determine the $f_r$ of each structure, which is the ideal status neglecting the stress generations and membrane deflections accompanying by the fabrication processes. The $f_r$ of fabricated sensor chips are located in the range of 87.6～111 kHz which is higher than the FEM results for 30～40 kHz. These differences are well consistent with the tendencies of membrane deflections of each structure. The stresses of each structure have been approximated by the calculations of axial and bending strain, which mainly determined by the thermal expansion differences between constitutive layers and process temperatures. Although the thermal stress approximated also appreciably influence on the frequency shifts, the primary effects on that are the membrane deflections of the corresponding structures. Since the process temperature of SOI wafer fabrications is sufficiently high and stress generations are larger than the other layers, the oxide inter-layer of the membrane is a decisive factor on the membrane deflections, and it principally

Copyright (C) 2006 NuriMedia Co., Ltd.

determines the frequency shift.

## References


Chinmulgund, M., Inturi, R. B. et al., 1995, "Effect of Ar Gas Pressure on Growth, Structure, and Mechanical Properties of Sputtered Ti, Al, TiAl, and Ti3Al Films," *Thin Solid Films*, Vol. 270, pp. 260～263.

Fitch, J. T., Bjorkman, C. H. et al., 1989, "Intrinsic Stress and Stress Gradients at the $SiO_2$/Si Interface in Structures Prepared by Thermal Oxidation of Si and Subjected to Rapic Thermal Annealing," *J. Vac. Sci. Technol. B*, Vol. 7, No. 4, pp. 775～781.

Gauthier, M. M., 1995, *Engineering Materials Handbook* (ASM desk edt.), Materials Park, OH.

Harms, U., Kempen L. et al., 1998, "Influence of Stress in Thin Film Modulus Measurements by the Vibrating Reed Technique," *Thin Solid Films*, Vol. 323, pp. 153～157.

Harris, C. M., 1995, *Shock and Vibration Handbook* ($4^{th}$ Edt.), McGraw-Hill, New York, pp. 7.25～7.49.

Hess, P., 1996, "Laser Diagnostics of Mechanical and Elastic Properties of Silicon and Carbon Films," *Appl. Surf. Sci.*, Vol. 106, pp. 429～437.

Hwang, H. Y., Kim, Y. K., Kim, C., Kwon, Y. -D. and Choi, W., 2003, "Thermo-Viscoelastic Residual Stress Analysis of Metal Linear-Inserted Composite Cylinders," *KSME International Journal*, Vol. 17, No. 2, pp. 171～180.

Irene, E. A. and Tierney, E., 1982, "A Viscous Flow Model to Explain the Appearance of High Density Thermal $SiO_2$ at Low Oxidation Temperatures," *J. Electrochem. Soc.*, Vol. 129, No. 11, pp. 2594～2597.

Katz, A. and Dautremont-Smith, W. C., 1990, "Stress Measurements of Pt/Ti/InP and Pt/Ti/$SiO_2$/InP Systems : In Situ Measurements Through Sintering and After Rapid Thermal Processing," *J. Appl. Phys.*, Vol. 67, No. 10, pp. 6237～6246.

Kim, M. T., 1996, "Influence of Substrates on the Elastic Reaction of Films for the Microindentation Tests," *Thin Solid Films*, Vol. 283, pp. 12～16.

Low, T. S. and Guo, W., 1995, "Modeling of' a Three-Layer Piezoelectric Bimorph Beam with Hysteresis," *J. MEMS*, Vol. 4, No. 4, pp. 234～237.

Mo, Y., Tanaka, T., Inoue, K. et al., 2003, "Front-End Processor Using BBD Distributed Delay-Sum Architecture for Micromachined Ultrasonic Sensor Array ," *J. MEMS*, Vol. 12, No. 12, pp. 506～512.

Nayfeh, S. A., 0000, "Damping of flexural vibration in the plane of lamination of elastic-viscoelastic sandwich beams," *J. Sound and Vibration*, in press.

Okuyama, M., 2001, "Electronic devices using the ferroelectric thin film," *T. IEE Japan*, Vol. 121-E, pp. 537～541. (in Japanese).

Pietrzakowski, M., 2001, "Active Damping of Beams by Oiezoelectric System : Effects of Bonding Layer Properties," *Int. J. Solids and Structures*, Vol. 38, pp. 7885～7897.

Sengupta, S. S., Park, S. M. et al., 1998, "Origins and Evolution of Stress Development in Sol-Gel Derived Thin Layers and Multideposited Coatings of Lead Titanate," *J. Appl. Phys.*, Vol. 83, No. 4, pp. 2291～2296.

Spierings, G. A. C. M., Dormans, G. J. M. et al., 1995, "Stresses in Pt/Pb(Zr, Ti)$O_3$/Pt Thin-Film Stacks for Integrated Ferroelectric Capacitors," *J. Appl. Phys.*, Vol. 78, No. 3, pp. 1926～1933.

Sze. ed, S.M., 1994, *Semiconductor Sensors*, Wiley Inter-Science, New York.

Timosenko, S. and Woinowsky-Krieger, S., 1959, *Theory of Plates and Shells* ($2^{nd}$ Edt.), McGraw-Hill, New York, pp. 30.

Townsend, P. H., Barnett D. M. et al., 1987, "Elastic Relationships in Layered Composite Media with Approximation for the Case of Thin Films on a Thick Substrate," *J. Appl. Phys.*, Vol. 62, No. 11, pp. 4438～4444.


Copyright (C) 2006 NuriMedia Co., Ltd.